

Article

# Teleconnections between Monthly Rainfall Variability and Large-Scale Climate Indices in Southwestern Colombia

Teresita Canchala <sup>1,\*</sup>, Wilfredo Alfonso-Morales <sup>2</sup>, Wilmar Loaiza Cerón <sup>3</sup>,  
Yesid Carvajal-Escobar <sup>4</sup> and Eduardo Caicedo-Bravo <sup>2</sup>

<sup>1</sup> Water Resources Engineering and Soil Research Group (IREHISA), School of Natural Resources and Environmental Engineering, Universidad del Valle, Cali 25360, Colombia

<sup>2</sup> Perception and Intelligent Systems Research Group (PSI), School of Electrical and Electronic Engineering, Universidad del Valle, Cali 25360, Colombia; wilfredo.alfonso@correounivalle.edu.co (W.A.-M.); eduardo.caicedo@correounivalle.edu.co (E.C.-B.)

<sup>3</sup> Faculty of Humanities, Department of Geography, Universidad del Valle, Cali 25360, Colombia; wilmar.ceron@correounivalle.edu.co

<sup>4</sup> Faculty of Engineering, Natural and Environmental Resources Engineering School (EIDENAR), Universidad del Valle, Cali 25360, Colombia; yesid.carvajal@correounivalle.edu.co

\* Correspondence: teresita.canchala@correounivalle.edu.co; Tel.: +57-311-7474929

Received: 2 June 2020; Accepted: 25 June 2020; Published: 29 June 2020



**Abstract:** Given that the analysis of past monthly rainfall variability is highly relevant for the adequate management of water resources, the relationship between the climate-oceanographic indices, and the variability of monthly rainfall in Southwestern Colombia at different time scales was chosen as the research topic. It should also be noted that little-to-no research has been carried out on this topic before. For the purpose of conducting this research, we identified homogeneous rainfall regions while using Non-Linear Principal Component Analysis (NLPCA) and Self-Organizing Maps (SOM). The rainfall variability modes were obtained from the NLPCA, while their teleconnection in relation to the climate indices was obtained from Pearson's Correlations and Wavelet Transform. The regionalization process clarified that Nariño has two regions: the Andean Region (AR) and the Pacific Region (PR). The NLPCA showed two modes for the AR, and one for the PR, with an explained variance of 75% and 48%, respectively. The correlation analyses between the first nonlinear components of AR and PR regarding climate indices showed AR high significant positive correlations with Southern Oscillation Index (SOI) index and negative correlations with El Niño/Southern Oscillation (ENSO) indices. PR showed positive ones with Niño1 + 2, and Niño3, and negative correlations with Niño3.4 and Niño4, although their synchronous relationships were not statistically significant. The Wavelet Coherence analysis showed that the variability of the AR rainfall was influenced principally by the Niño3.4 index on the 3–7-year inter-annual scale, while PR rainfall were influenced by the Niño3 index on the 1.5–3-year inter-annual scale. The El Niño (EN) events lead to a decrease and increase in the monthly rainfall on AR and PR, respectively, while, in the La Niña (LN) events, the opposite occurred. These results that are not documented in previous studies are useful for the forecasting of monthly rainfall and the planning of water resources in the area of study.

**Keywords:** Southwestern Colombia; nonlinear principal component analysis; monthly rainfall variability; climate-oceanographic indices; wavelet analysis

## 1. Introduction

Knowledge of the spatio-temporal variability of rainfall is critical for the appropriate management of water resources [1]. For this reason, it is necessary to analyze the historical records of rainfall regimes and their relationships with different climate variability scales. The joint analysis of these variables provides useful information for the reliable forecasting of future scenarios of both the hydrological cycle and the impacts on the availability of the water resource at different scales [2,3]. Climate variability is manifested through changes in recurrent and oscillatory patterns of climatic variables, such as sea level pressure (SLP) and sea surface temperature (SST), which act to different scales of time (inter-annual to multi-decadal) [4]. The interaction of oceanic-atmospheric variables is closely connected with the long-term variability of rainfall. Moreover, there are climate indices that summarize the information fundamental of the ocean and atmosphere, and they are commonly used to explain the variability of the hydro-climatic process [5].

The climate variability of South America (SA) has a connection with the large-scale climatic phenomenon named El Niño/Southern Oscillation (ENSO). ENSO has two phases: El Niño (EN) and La Niña (LN), which denote that SST in the Tropical Pacific Ocean (TPO) is warmer and colder than average, respectively. This phenomenon affects the rainfall variability in tropical regions; and, in its extreme phases, can lead to drought and floods causing adverse socio-economic effects in a given area [6]. In Colombia, several studies claim that the EN (LN) episodes have connections with the decrease (increase) of rainfall, streamflows, and other hydro-climatic variables, predominantly in the central, northern, and western parts of the country [7–12]. However, the climatic variability of this region can also be modulated by local factors, such as the migration of the Intertropical Convergence Zone (ITCZ), the Chocó Low-Level Jet [13,14], the presence of the Andes Mountain Range [15], and the atmospheric rivers [16].

Colombia has regions with complex topographic conditions given the presence of the Andes Mountain Range [15], which can interact with the moisture that comes in from the tropical Pacific Ocean toward the continent, and the trade-winds that can contribute to the deep convection process [17]. Therefore, the rainfall patterns can change over small distances in the same region. For example, in some areas of SA, such as Ecuador, the Andes Mountain Range can modify the ENSO influence and show opposite effects in the coastal and Andean region of the country [18,19]. In this respect, Hurtado [20] in the sub-regional scale of Colombia, reported high variability of rainfall in small distances established by gradients in topographic features, mainly on the Pacific lowlands and on the mountain slopes. Studies have been carried out on different regions of the country, which have evaluated the relationships between several hydroclimatic variables and climate indices that are associated with ENSO [10–12,21–27]. Nevertheless, these teleconnections have not been studied in Southwestern Colombia so far, given that it lies close to TPO and the Andes Mountain, on the border with Ecuador [28], and they therefore offer complex topographic conditions.

In this regard, this research study aims to analyze the teleconnections between monthly rainfall and climate-oceanographic indices in southwestern Colombia. This research study is structured, as follows: Section 2 presents data and applied methods; Section 3 shows the results and discussion; and, Section 4 presents the main conclusions.

## 2. Data and Methods

### 2.1. Study Area

The research area is located in Southwestern Colombia (Department of Nariño), south of Colombian Biogeographic Choco, one of the most biodiverse regions of Colombia, and of the world (Figure 1). The Department of Nariño has an approximate area of 33,268 km<sup>2</sup>, and it has a geo-strategic position due to its proximity to the TPO and the presence of the Andes Mountain [28].

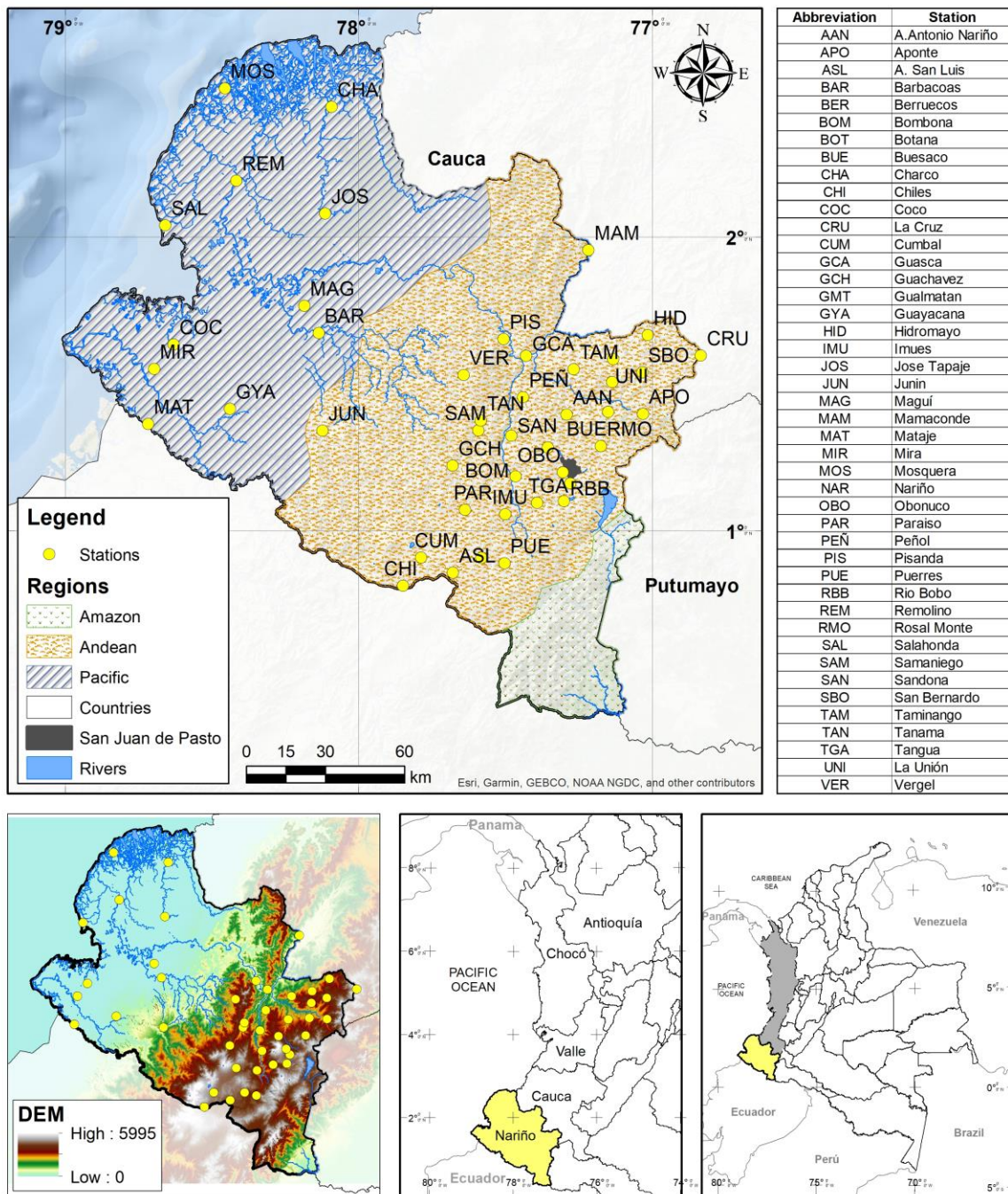


Figure 1. The geographic location of the study area and the distribution of the rainfall gauge stations.

### 2.2. Rainfall Dataset

We used monthly rainfall time series, from 1983 to 2016, which included the forty-four rainfall-gauge stations located in different zones in Nariño, as provided by Instituto de Hidrología, Meteorología y Estudios Ambientales (IDEAM) of Colombia. Table 1 presents the main features and descriptive statistical attributes of each rainfall gauge station. The monthly rainfall series presented missing data in the percentage, also specified in Table 1. Here, we estimated this data using non-linear principal component analysis (NLPCA), as suggested by Scholz et al. [29]. Refer to Canchala et al. [28] for further details regarding how missing data in Nariño using this non-linear approach was estimated.

After completing the procedure for each of the series, we calculated the accuracy using the Root Mean Square Error (*RMSE*)

$$RMSE = \sqrt{\frac{1}{n} \sum_{i=1}^n (r_i - o_i)^2} \quad (1)$$

where *r* is the reconstructed value, *o* indicates the observed value, and *n* refers to sample size.

**Table 1.** Description of the monthly rainfall dataset (1983–2016).

Gauge-Station	Cumulative (mm/Year)	Mean (mm/Year)	SD (mm/Year)	CV	Missing (%)
AAN	1189	98.10	71	0.73	0.00
APO	1540	72.50	116	0.90	0.00
ASL	873	128.60	43	0.60	0.00
BAR	6430	562.80	256	0.46	4.41
BER	1739	145.40	111	0.76	0.74
BOM	1039	86.30	61	0.71	0.25
BOT	917	76.30	40	0.53	0.74
BUE	1254	104.60	92	0.88	1.23
CHA	3603	301.60	148	0.49	6.86
CHI	1089	91.40	62	0.67	0.98
COC	2648	215.50	180	0.84	2.45
CRU	1330	75.20	91	0.82	0.98
CUM	892	138.10	48	0.64	0.00
GCA	582	77.50	46	0.95	0.00
GCH	1652	49.00	92	0.66	0.74
GMT	939	500.20	54	0.69	0.74
GYA	6006	110.30	224	0.45	2.21
HID	1334	83.50	88	0.80	0.49
IMU	1001	399.80	60	0.72	0.25
JOS	4784	726.60	222	0.56	2.70
JUN	8693	112.00	271	0.37	0.49
MAG	4852	164.60	237	0.58	3.43
MAM	1328	404.40	94	0.87	0.98
MAT	3437	107.50	197	0.68	9.07
MIR	2972	289.70	159	0.64	2.21
MON	3191	250.00	126	0.47	4.41
MOS	3575	267.80	198	0.65	3.19
NAR	1987	304.40	126	0.76	0.00
OBO	812	165.50	52	0.76	6.62
PAR	989	68.70	52	0.64	0.49
PEÑ	1102	82.40	65	0.72	0.00
PIS	1253	90.40	80	0.75	0.00
PUE	1025	105.60	49	0.58	0.00
RBB	1099	84.90	53	0.58	0.98
REM	2823	228.60	163	0.72	10.78
RMO	1346	91.70	90	0.81	0.98
SAL	1455	111.90	238	0.60	3.19
SAM	1455	396.50	98	0.81	0.00
SAN	1144	122.10	78	0.82	0.98
SBO	2007	167.00	117	0.70	0.49
TAM	1732	95.20	96	0.68	0.98
TAN	1342	140.90	80	0.71	0.98
TGA	1002	112.90	61	0.73	0.49
UNI	1983	83.80	115	0.70	0.49
VER	2554	214.80	145	0.68	3.68

### 2.3. Climate-Oceanographic Indices

Additionally, we selected eight monthly atmospheric and ocean time-series. This selection was performed while taking into account the results of previous research studies on teleconnections between the hydro-climatology of Colombia, and large-scale climate indices that have identified relationships with Southern Oscillation Index (SOI), Multivariate ENSO Index (MEI), Oceanic Niño Index (ONI), and SST in regions of the TPO (Niño1 + 2, Niño3, Niño3.4, Niño4) and Pacific Decadal Oscillation (PDO) [9–12,22–24,27,30–32]. These indices are available in the National Oceanic and Atmospheric Administration (NOAA) (<https://www.esrl.noaa.gov/psd/data/climateindices/list/>). SOI is a measure of the large-scale oscillations in air pressure that take place between the west and east of the TPO, and is estimated as the difference in the Sea Level Pressure (SLP) anomalies between Tahiti and Darwin. MEI is an index obtained from six variables over the TPO: SLP, winds, SST, air temperature, and cloudiness [33]. ONI corresponds to the three-month moving average of SST anomalies on the Niño3.4 region [34]. Niño1 + 2, Niño3, Niño3.4, and Niño4 were calculated with the average of SST in the boxes 0–10° S, 90°–80° W, 5° S–5° N, 90°–150° W, 5° N–5° S, 170°–120° W, and 5° N–5° S, 160° E–150° W, respectively. The PDO is the principal component time series of the leading empirical orthogonal function mode of the SST anomalies in the Northern Pacific Ocean, poleward of 20° N [35].

### 2.4. Regionalization of Monthly Rainfall

In this study, we established homogeneous rainfall regions in Nariño through the combination of two non-linear methods: NLPCA, and Self-Organized Feature Map (SOM), as efficient approaches to identify clusters with similar features of rainfall. NLPCA is a multi-layer feedforward network with a self-associative topology, also known as auto-encoder [29], which reduces the dimensionality of the dataset extracting its main features [36]. SOM is an Artificial Neural Network (ANN) based unsupervised clustering algorithm, introduced by Kohonen [37], which approximates the probability density function of the input data. It preserves the neighborhood properties and local resolution of the input space proportional to the data distribution [38,39]. Due to the robustness of SOM, its applications are focused on clustering and the modeling of hydrological datasets, such as precipitation, streamflow, runoff, and others [40]. Lin and Chen [41] and Chen et al. [42] have evidenced the advantage of SOM over conventional regionalization methods. Thus, the input data with 44-gauge stations into a temporal series of 408 months (34 years), required the use of NLPCA to reduce the dimensionality of the dataset to five non-linear components using a network with a (408-200-25-5) topology. These five nonlinear components were then used as input of SOM to capture a profile of the homogeneous areas and obtain a classification of gauge stations. The grid obtained from SOM in the output layer corresponds to 25 nodes (5 × 5 cells), which was enough to split the data-gauge stations. Finally, we validated the identified clusters through Discriminant Analysis (DA), as developed by Fisher [43]; more details about this test are described in Phalm et al. [44]. We used the Kolmogorov–Smirnov (K–S) test to measure the homogeneity of the identified sub-regions. This non-parametric test allows us to infer that the subjacent distribution of two datasets has significant differences [45,46].

### 2.5. Nonlinear Principal Component Analysis

The NLPCA is a non-linear generalization of principal component analysis (PCA) [47]. Given that the NLPCA generalizes the components, including lines and curves, it, therefore, depicts the structure of the data in curved subspaces [48]. NLPCA, as developed by Hsieh. [47] and Scholz. [48], uses the multi-layer perceptron of an auto-associative topology, known as a bottleneck (or auto-encoder). Figure 2 shows the neural network (NN) model for calculating NLPCA.

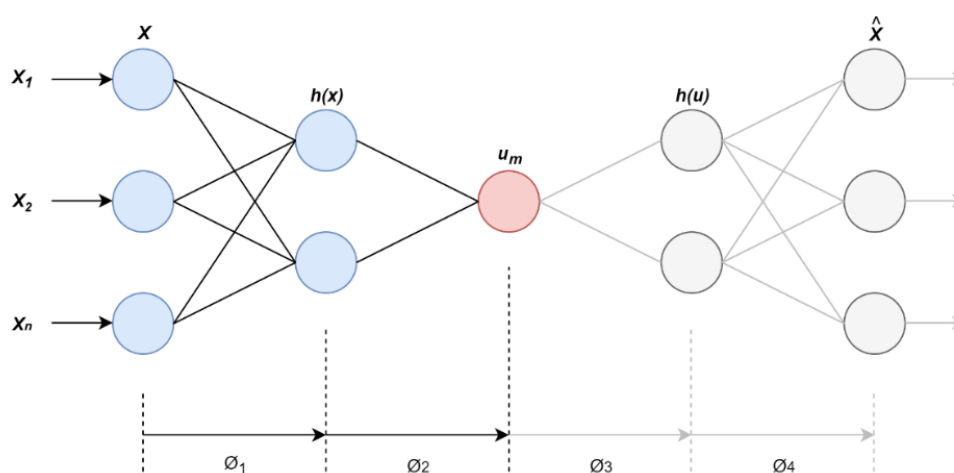


**Figure 2.** Diagram of non-linear principal component analysis (NLPCA) with a (3-2-1-2-3) network topology. This diagram shows 3 “hidden” layers of “neurons” (indicated by circumferences) inserted between the input layer  $x$  on the left and the output layer  $\hat{x}$  on the right.  $h(x)$  is the encoding layer,  $u$  is the bottleneck layer and  $h(u)$  is the decoding layer.  $\phi_1$ ,  $\phi_2$ ,  $\phi_3$ , and  $\phi_4$  are the transfer functions. Adapted from Kenfack et al. [49].

The dimensions of  $x$  and  $h(x)$  are  $n$  and  $m$ , respectively. Where  $x$  is the input column vector of length  $n$  and  $m$  is the number of hidden neurons in the encoding and decoding layers for  $u$ . More details about NLPCA are available in Scholz [50] and Hsieh [47].

NLPCA is a non-linear statistical method that is employed to analyze hydro-climatological, meteorological, and oceanographic data, such as rainfall, streamflow, or oceanographic variables [28,36,47,49,51–53]. It has been widely used in recent years due to its advantages (over PCA) in the maximization of the explained global variance [47], most notably when non-linear processes, such as the rainfall distribution, rainfall clustering, atmospheric circulation regimes, among others, are involved [53,54]. Its objective is to obtain some non-linear components that explain the main modes of the variability of the original dataset that offer the least loss of information. This research uses the Non-linear PCA toolbox (<http://www.nl pca.org/matlab.html>) to obtain the hierarchically-ordered features by sequentially training and calculating the explained variance of each of the NLPCs. The NLPCA method helps to establish the dominant modes of variability of the monthly rainfall of Nariño in each of the clusters previously identified. The best architecture is based on the best performance, in terms of the highest percentage of explained variance.

Before performing monthly NLPCA for each group, we turned the rainfall values into anomalies by subtracting each month’s mean.

## 2.6. Teleconnections

We applied the cross-correlations through Pearson Correlations, using a 12-month maximum lag, and taking into account that the climate indices precede the monthly rainfall, in order to measure the degree of correlation between the main modes of variability of monthly rainfall and the climate-oceanographic indices, as well as the persistence of the relationship. The student t-test helped to define the statistical significance with a confidence value of 95% ( $\alpha = 0.05$ ).

Once the climatic indices with the highest incidence on the NLPCs were determined, we estimated the energy spectrum by wavelet transform to verify the spatio-temporal variability of rainfall, and the cross-wavelet analysis to compare two-time series. The hydro-climate field widely used the Wavelet Transform Methodology for different purposes, such as to: analyze the ENSO influence over the spatio-temporal variability of droughts [12]; study rainfall extremes and its relationship with climate indices [55]; identify teleconnections between monthly streamflow and climate indices [11,27]; and, describe the variability in annual streamflows [56]. In this regard, we used Morlet’s Wavelet to obtain

the time-frequency representation of NLPCs following the methodology presented by Grinsted et al. [57] and the computational procedure proposed by Torrence and Compo [58]. To avoid spectral leakage and implement the Wavelet Transform, the time-series was filled with zeros to twice the data length. The wavelet function in each scale is standardized to get the energy unit, ensuring the ability to compare the wavelets with others. For more detailed wavelet theory, refer to Torrence and Compo [58]. The Global Wavelet Spectrum (GWS) allows for a better visualization of the distribution of power linked to the frequencies in the climate signals and ensures a better detection of fluctuation/oscillation. GWS is the time mean of all local Wavelet Power Spectrum (WPS) and it is explained with an equation (22) in Torrence and Compo [58].

The Wavelet Coherence (WTC) allows us to compare two-time series (NLPCs vs. climate-indices), due to the fact that there is a correlation coefficient that is estimated in time and space frequency. According to Torrence and Webster [59],  $X(t)$  and  $Y(t)$  series are given, with Wavelet Transforms,  $W^X(t, s)$  and  $W^Y(t, s)$ , the WTC can be defined as

$$R_n^2(s) = \frac{|\langle s^{-1} W^{XY}(t, s) \rangle|^2}{\langle s^{-1} |W^X(t, s)|^2 \rangle \langle s^{-1} |W^Y(t, s)|^2 \rangle} \quad (2)$$

where  $\langle \rangle$  is a smoothing operator,  $W^{XY}(t, s) = W^X(t, s)W^{Y*}(t, s)$  is the cross-wavelet spectrum, (\*) indicates the conjugated complex,  $R_n^2$  can range from 0 to 1. 0 designates no-correlation between the two-series that are compared, and 1 indicates a perfect correlation. Monte Carlo methods help to estimate the statistical significance of the WTC. More details regarding the estimation of WTC's are available in Grinsted et al. [57].

### 3. Results and Discussion

#### 3.1. Missing Data Estimation

Figure 3 shows the recovery of missing data from the Remolino (REM) gauge station, which has the most missing data (see Table 1). The results of the estimation of all stations' missing data are available in Canchala et al. [28]. The best topology to recover data was with a network (45-44-45). The RMSE in the estimation of missing data corresponds to 9.8 mm/month.

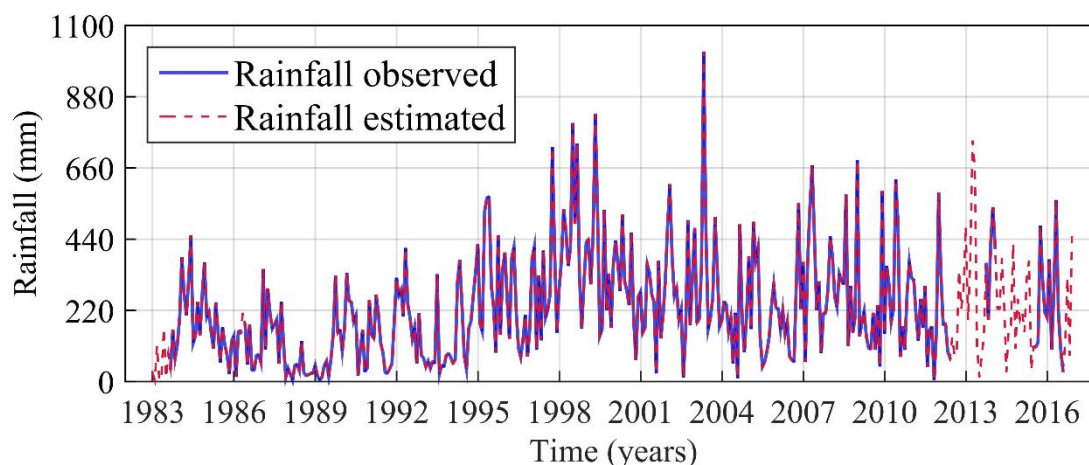


**Figure 3.** Time series rainfall of Remolino (REM) gauge station: observed vs. estimated.

### 3.2. Regionalization of Monthly Rainfall

The results of the non-linear approach for rainfall regionalization using NLPCA and SOM showed that Nariño has two clusters: the Andean Region (AR) and the Pacific Region (PR), each one with thirty-three and eleven-gauge stations, respectively (See Figure 4a). The Monopamba (MON) gauge station had to be removed from the analysis due to it is producing noise in the SOM study.

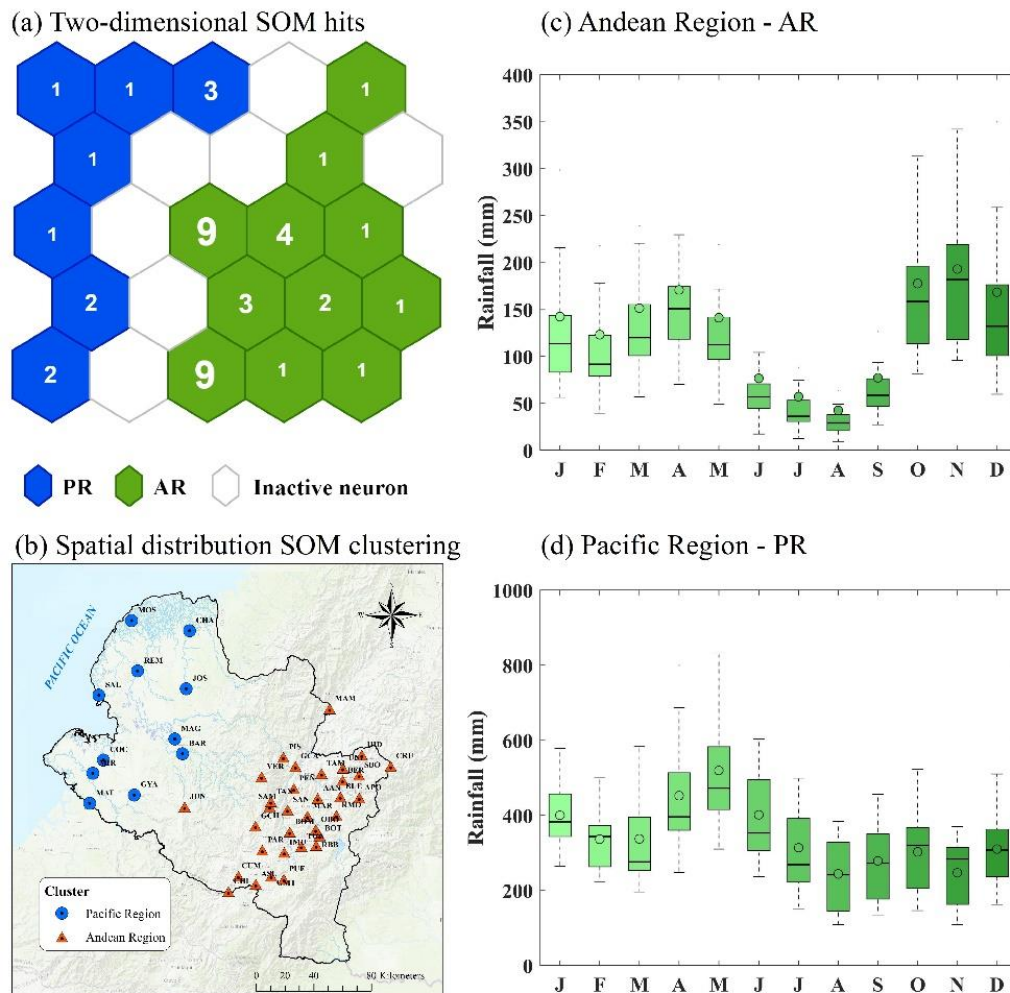
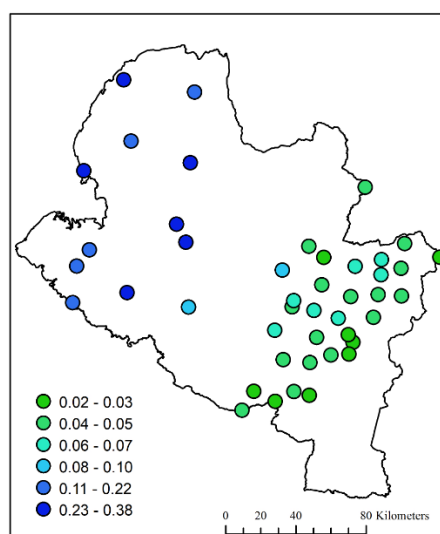


Figure 4. Regionalization of monthly rainfall in Southwestern Colombia.

The validation of the homogeneity of climatic regions, using the Fisher’s Discriminant Analysis [43], showed a 100% AR and PR classification accuracy. Besides, the K–S test allowed for us to verify the statistical significance of the identified regions, by assuming the null hypothesis that the distribution is the same [45,46]. This test showed a  $p$ -value  $< 0.05$ , indicating that the precipitation regimes in the regions are different. Figure 4b presents the spatial distribution of the forty-four gauge stations, organized according to the regionalization results. The main feature of rainfall in AR is that it records a bimodal annual cycle with an average monthly rainfall of about 130 mm/month (Figure 4c), whereas the PR shows a unimodal yearly cycle with an average monthly rainfall of about 350 mm/month (Figure 4d). For a better understanding of the spatial variability of rainfall anomalies in the two regions, refer to Figure 5, where you can find the first spatial pattern that was obtained from NLPCA that clearly shows two different rainfall patterns over the AR and PR.



**Figure 5.** The first spatial pattern of monthly rainfall in Southwestern Colombia.

### 3.3. Nonlinear Principal Component Analysis

The NLPCA results for two clusters, as previously identified, indicate two significant NLPCs for the AR, and one significant NLPC for the PR. The NLPCs explained around 75% and 48% of the Variance of the original data for AR and PR, respectively. We tested different topologies (see Table 2) to determine which one obtained the highest percentage of explained variance. The best result for AR was found with a (33-25-15-2-15-25-33) network topology, whereas the best outcome for PR was found with a (11-8-5-1-5-8-11) network topology. The components followed a hierarchical order, with a weight decay coefficient of 0.01 and 5000 iterations. The other parameters kept their default values.

**Table 2.** Topologies evaluated for the selection of the best ANN and the explained variance of the nonlinear components in each region. The best ANN topologies are in bold.

Region	Topologies	Explained Variance (%)		
		NLPC1	NLPC2	Total
AR	33-30-15-2-15-30-33	57.41	17.43	74.84
	<b>33-25-15-2-15-25-33</b>	<b>56.7</b>	<b>18.67</b>	<b>75.37</b>
	33-20-15-2-15-20-33	54.66	17.69	72.35
PR	<b>11-8-5-1-5-8-11</b>	<b>48.08</b>		<b>48.08</b>
	11-7-5-1-5-7-11	47.99		47.99
	11-6-5-1-5-6-11	47.88		47.88

Figure 6a indicates the time series of the first NLPC for AR (NLPC1-AR). Positive (negative) values for the NLPC1-AR include periods: 1988–1989, 1998–1999, 2000–2001, 2007–2008, 2008–2009, 2010–2011, and 2011–2012 (1987–1988, 1991–1992, 1997–1998, 2009–2010, and 2015–2016). Likewise, Figure 6b shows the time series of the second NLPC for AR (NLPC2-AR). Positive (negative) values for the NLPC2-AR include periods: 1985–1986, 1988–1989, 1998–1999, and 2011–2012 (1991–1992, 1997–1998, 2002–2003, 2009–2010, and 2015–2016). These positive (negative) periods of NLPC1-AR and NLPC2-AR correspond to the LN (EN) episodes, which were registered by Trenberth [60] and Tedeschi et al. [61]. On the other hand, Figure 6c shows the time series of the first NLPC for PR (NLPC1-PR), representing the primary mode of variability in the coastal region of Nariño. Negative (positive) values for the NLPC1-PR were registered during periods 1985–1986, 1988–1989, and 2011–2012 (1997–1998 and 2015–2016), which match with LN (EN) episodes.

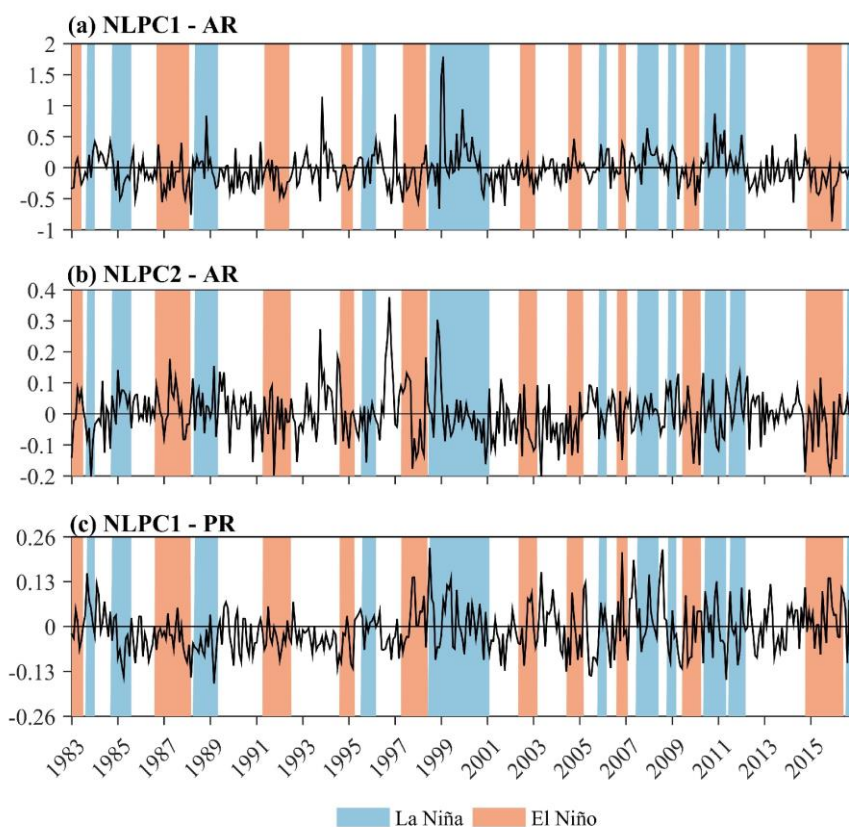


**Figure 6.** The 1983–2016-time series of the NLPCs for Andean Region (AR) and Pacific Region (PR): (a) NLPC1-AR, (b) NLPC2-AR, and (c) NLPC1-PR.

In SA, the establishment of an LN (EN) episode occurred with decreases (increases) of rainfall over the west coast of Ecuador, southern and southeastern of the continent, and increases (decreases) of them over the north and northeastern of SA [61,62]. Moreover, in the western, central, and northern territories of Colombia, LN is characterized by high and intense rainfall, increased streamflows, and progressive flooding [8,63,64]. In contrast, the pattern EN is related to an increase in the average air temperature, a decrease in rainfall, and a reduction in the average flow of the rivers [8,65]. This behavior is a characteristic of large areas of the Caribbean, Andean, and North Pacific Regions. Moreover, in the South Pacific Region, Southwestern Colombia, the Amazon, and some areas of the Piedmont Plains, the establishment of EN (LN) events is associated with increases (decreases) in rainfall [7].

Hence, the results registered in AR (Figure 6a,b) and PR (Figure 6c) are consistent with the above-mentioned, given that the rainfall in these two sub-regions recorded opposite effects when EN and LN events occurred. As an example, the monthly rainfall in AR, decreases when an EN event is registered, while the PR increases. In contrast, when the LN event occurred, the rainfall in AR and PR increases and decreases, respectively. In Colombia, the 1997–1998 EN event is considered to have had the highest intensity and spatial amplitude with devastating effects on different economic sectors. These generated phenomena, such as heatwaves, droughts, forest fires, as well as diminished rainfall and streamflows in some regions; while others recorded more torrential rainfalls, landslides, and floods [66]. In this regard, the registered behavior for AR (PR) NLPCs showed negative (positive) anomalies during the 1997–1998 EN event (See Figure 6). Meanwhile, the effects of this EN event in PR were similar to those that occurred in 1997–1998 in Ecuador’s coastal region (a region that borders with the PR of Nariño), which produced significant positive rainfall anomalies, affecting different economic sectors [67]. These ENSO events have been cataloged by the NOAA as a strong event.

According to Quishpe-Vásquez et al. [68], during the EN events, the trade winds weakens along the equator; therefore, the Walker circulation also weakens as atmospheric pressure in western OPT

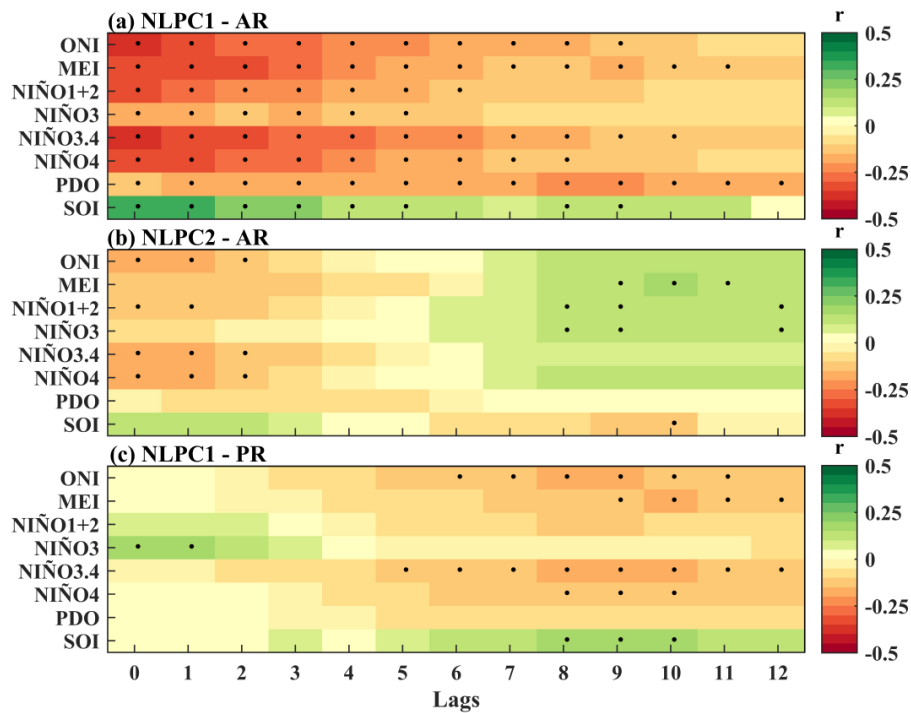
increases, while the atmospheric pressure in the Eastern Pacific decreases. It caused a displacement of the warm waters of the Central Pacific to the east, and the weakening of the Humboldt current [69]. Furthermore, the ITCZ movement to the south caused heavy rainfall on the coast of Ecuador [70,71]. The opposite effect can occur with LN events; for example, the 2010–2011 LN event in Nariño showed positive (negative) anomalies for AR (PR). The positive anomalies in AR match anomalies registered in a significant part of Colombia, which recorded extreme precipitation and river discharges that affected approximately 9% of the country's population [65]. In contrast, the negative anomalies in PR match anomalies registered on neighboring regions of Colombia, specifically in the Ecuadorian coast where the drought is associated to the LN event [72].

These results have shown the importance of analyzing the monthly rainfall variability to regional scale and study its relationships with ENSO indices, when considering that, despite there being rainfall regionalization studies throughout the country, such as those developed by Guzman et al. [73], and Estupiñan [74], which coincide with the regionalization performed here, it is the first time that it found significant differences in the relationships between ENSO events and the Southwestern Colombia rainfall, even at very short distances between these sub-regions. Therefore, in the next section, we consider it relevant to study the teleconnections with the different ENSO indices to identify the different time scales required to improve understanding of the findings found so far.

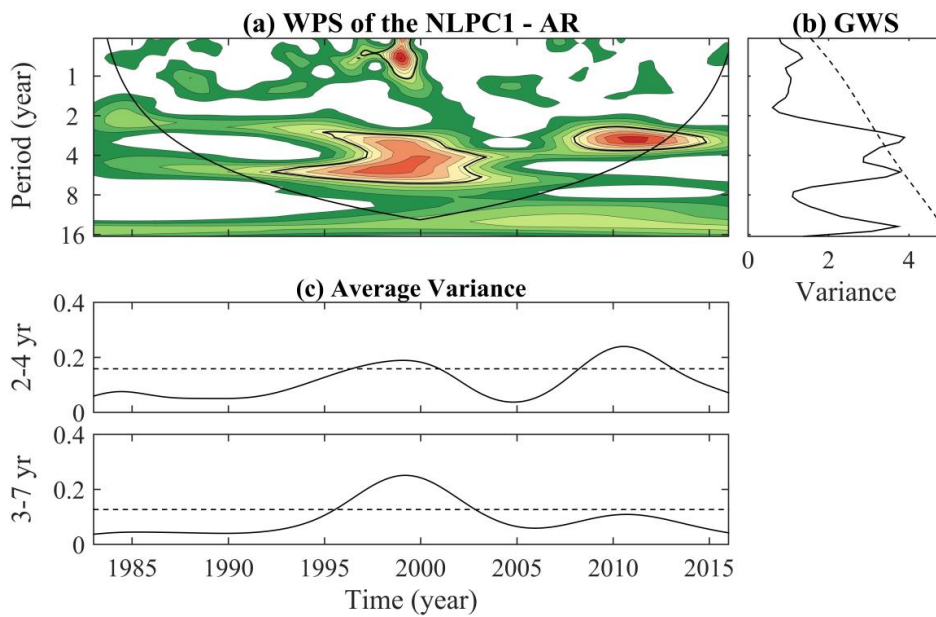
#### 3.4. Teleconnections

The degree of the relationships between the main modes of variability of monthly rainfall in the sub-regions AR and PR and the climate-oceanographic indices was studied while using Pearson's Correlation Analysis. Figure 7 shows the cross-correlation coefficients between the NLPC's of the two sub-regions of Nariño and the climate-oceanographic indices at lag = 0 to lag = 12. The cross-correlations for NLPC1-AR (Figure 7a) showed negative (positive) correlations with ONI, MEI, Niño1 + 2, Niño3, Niño3.4, Niño4, and PDO (SOI) in all of the lags studied, demonstrating that the inverse (direct) relation with oceanic (atmospheric) indices is persistent in this period. The correlations that were statistically significant are shown with a dot in the Figure 7. The highest partial cross-correlation coefficients were: lag = 0 (ONI, Niño1 + 2, Niño3, Niño3.4, and Niño4), lag = 1 (SOI), lag = 2 (MEI), and lag = 9 (PDO). Meanwhile, not all of the relationships between NLPC2-AR and climate indices that are shown in Figure 7b were statistically significant. The highest positive (negative) correlations at lag = 0 were registered with SOI (ONI, Niño3.4, and Niño4), lag = 1 (Niño3.4), lag = 9 (Niño3), and lag = 10 (SOI). In contrast, the cross-correlations for NLPC1-PR (Figure 7c) at lag = 0 showed positive correlations and were statistically significant only with the Niño3 index. The highest partial cross-correlation coefficients for PR were: lag = 0 (Niño3), lag = 8 (ONI), lag = 9 (Niño1 + 2, Niño3.4, Niño4, and SOI), and lag = 10 (MEI).

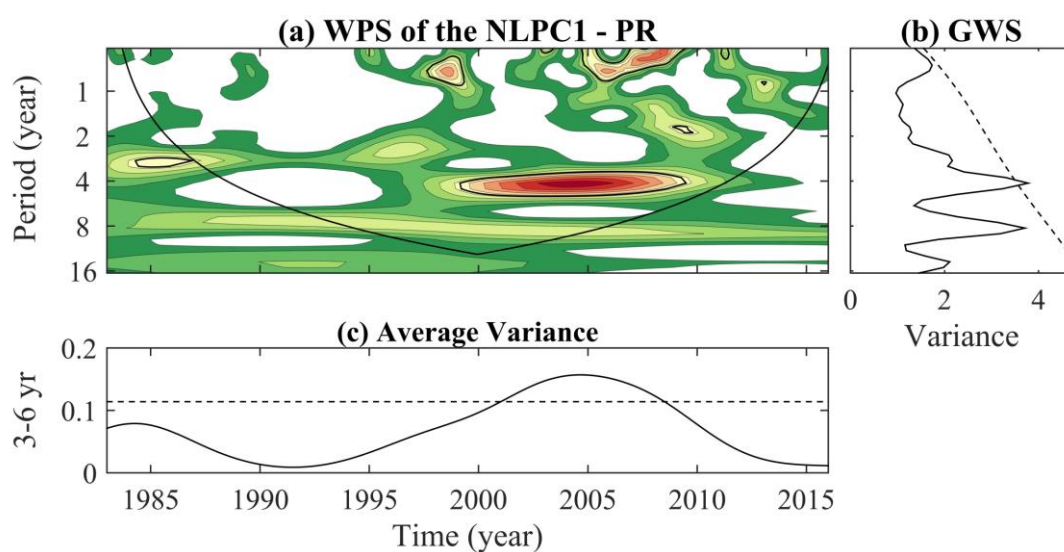
We used the wavelet transform analyses to understand the variability of monthly rainfall in terms of time and frequency with the purpose of studying the teleconnections between AR and PR rainfall with climate-oceanographic indices in their entirety. The Wavelet Analysis applied to NLPC1-AR (Figure 8a), showed a strong WPS on the inter-annual scales of the 2–4-year and 3–7-year periods, during 1992–2003, and 2008–2015, respectively. Meanwhile, the WPS of the NLPC2-AR indicates a significant and robust variability on the inter-annual band of a 2–4-year period, during 1993–2003 (the results are not shown here). The WPS of the NLPC1-PR showed that the concentrated power occurred on the 3–6-year scale during 1998–2010 (Figure 9a). The GWS of the NLPC1-AR (NLPC1-PR) showed 2–4- and 3–7- (3–6-) year inter-annual peaks with a significant level of 5% (See Figures 8b and 9b).



**Figure 7.** Cross-correlograms between climate-oceanographic indices and: (a) NLPC1-AR, (b) NLPC2-AR, and (c) NLPC1-PR. The statistically significant correlations are shown with a dot (significance level of 0.05 is  $\pm 0.128$ ).



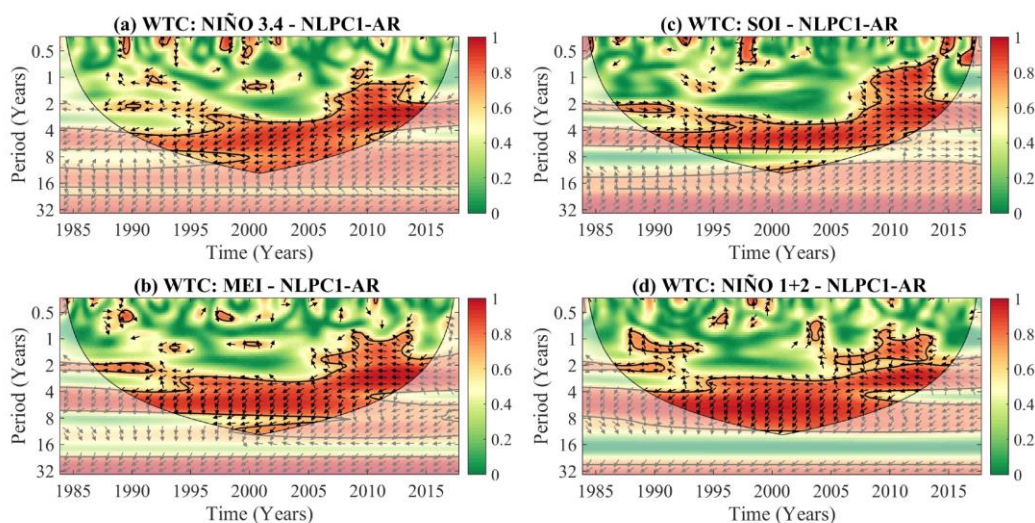
**Figure 8.** (a) Wavelet power spectrum (WPS) of NLPC1-AR. The closed contours encompass significant variations with confidence levels of 95%; Under the U-shaped curve, the region where the edge effects are important can be noted; (b) Global Wavelet Spectrum (GWS); and, (c) 2–4- and 3–7-year Scales-Averaged Power (SAP) of the time series.



**Figure 9.** (a) Wavelet Power Spectrum (WPS) of NLPC1-PR. The closed contours encompass significant variations with a confidence level of 95%; Under the U-shaped curve, the region where the edge effects are important can be noted; (b) global wavelet spectrum (GWS); and, (c) 3–6-year Scales-Averaged Power (SAP) of the time series.

The Scale-Averaged Wavelet Power (SAP) scales correspond to 2–4- and 3–7-year scales for NLPC1-AR (Figure 8c), and 3–6-year scales for NLPC1-PR (Figure 9c). Overall, NLPC1-AR showed significant time oscillations of the SAP (at variance units) and of the series on the 2–4-(3–7-) year scale for the 1996–2001 and 2008–2013 (1995–2003) periods. The SAP series for the 3–6- year period of NLPC1-PR registered significant oscillations during 2001–2008.

Figure 10 depicts the Wavelet Coherence results for AR rainfall and the climate-oceanographic indices that best explain the variability of rainfall. The coherence wavelet between NLPC1-AR and Niño1 + 2 and Niño3 (ONI, MEI, Niño3.4, and Niño4) indices showed similar relationships that were mainly focused at a time scale of 3–8-(3–7-) years from 1989 to 2011 (1989 to 2011), with a phase difference of  $-145^\circ$  to  $180^\circ$  ( $-135^\circ$  to  $180^\circ$ ) (refer to Figure 10a,b, respectively). The  $-145^\circ$  and  $135^\circ$  phase relationship for the 3–8-year and 3–7-year interannual scale shows that the EN (LN) event either led to dry (wet) conditions for approximately 4–9 months and 5–11 months, respectively. The  $180^\circ$  phase difference that shows the negative (positive) rainfall anomalies have a synchronous relationship with the mature phase of the EN (LN) events. Besides, there are significant coherences between the SOI index and NLPC1-AR for a 3–7-year inter-annual scale (1989–2011), also present in the same  $0^\circ$  to  $45^\circ$  phase (Figure 10c). A  $45^\circ$  phase relationship indicates that the negative (positive) rainfall anomalies were either led by negative (positive) SOI index by approximately 5–11 months, whereas  $0^\circ$  indicates a synchronous relationship between both series. Meanwhile, the Wavelet Coherence between the NLPC2-AR and Niño1 + 2, Niño3.4, Niño4, and ONI indices showed similar relationships (Figure 10d only shows El Niño1 + 2). The main ones were at a time scale of 1.5–3-years from 1995 to 2003 with a phase difference of  $160^\circ$  to  $180^\circ$ , establishing a phase difference around 1–2 months. Therefore, this implies that EN (LN) event preceded dry (wet) conditions by approximately 1–2 months.



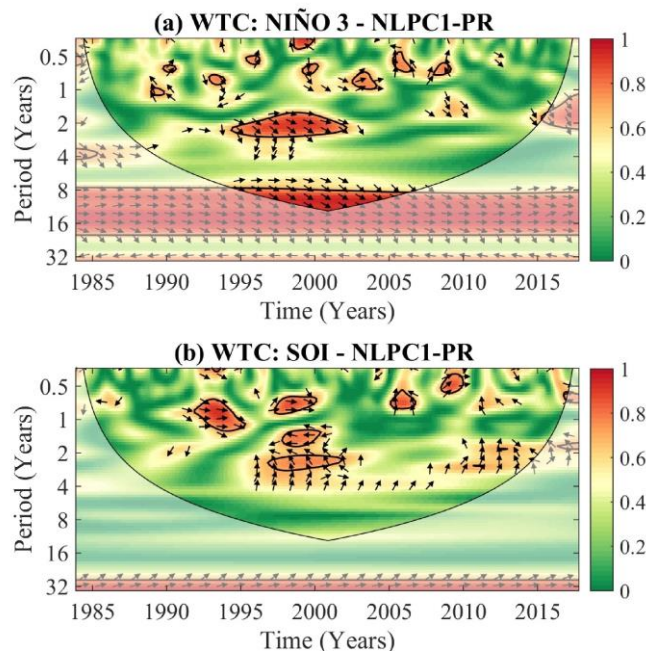
**Figure 10.** Wavelet transforms coherence between the NLPCs series of AR and climate-oceanographic indices: NLPC1-AR (a) Niño3.4, (b) MEI, (c) SOI, and (d) Niño1 + 2 (NLPC2-AR). The closed contours indicate the squared Wavelet Coherence. The region where the edge effects are significant is under the cone of influence. The arrows denote phase differences: in-phase ( $0^\circ$ ), arrows point out to the right; out of phase ( $180^\circ$ ), arrows point out to the left; the first-time series leads the second by  $90^\circ$ , pointing down; and, the first-time series, the second one by  $90^\circ$ , pointing upwards.

Figure 11a,b show the Wavelet Coherence between the NLPC1-PR with Niño3 and SOI indices, respectively. Figure 11a showed significant relationships on the 1.5–3-year interannual scale from 1995 to 2003, with a phase relationship of  $10^\circ$  to  $45^\circ$ , indicating an approximate phase difference of 1–5 months. This implies that there was an increase (decrease) in the SST in the Niño3 region, which led to positive (negative) rainfall anomalies in this region. Furthermore, it shows an 8–12-year decadal-scale from 1995 to 2006, with a  $-45^\circ$  phase relationship, indicating that PR rainfalls occur after fluctuations in Niño3 by around 12–18 months. Furthermore, the relationship between SOI index and NLPC1-PR (Figure 11b) did not help to establish a significant coherence wavelet, with the exception of the period of 1992 to 1995, where a phase relationship of  $0^\circ$  to  $10^\circ$  at a 0–1.5-year inter-annual scale was evidenced, which implied lags of 0–1 month between them.

Overall, the cross-correlation analysis (Figure 7) helped to establish that the rainfall of the AR represented in the primary variability mode (NLPC1-AR), has a meaningful teleconnection with oceanic macroclimatic indices linked to the ENSO phenomenon. In contrast, the PR rainfall of represented in NLPC1-PR has a weak teleconnection with climate indices that were studied here. The weak direct relationship is mainly associated to the sea surface temperature of the Niño3 region, showing that the ENSO phenomenon does not strongly affect the variability of rainfall in the coastal region of Nariño. These results from the cross-wavelet analysis (Figures 10 and 11) showed that there is a strong (weak) relationship inverse (direct) between AR (PR) rainfall and the SST in Niño3.4, and Niño4 (Niño3) on the 3–7-(1.5–3)-year inter-annual scale. Besides helping to establish that the warm (cold) phase of ENSO precedes dry(wet) conditions by approximately 5–11 months in AR, while the results also helped establish that the warm (cold) phase of ENSO precedes wet(dry) conditions by around 1–5 months in PR.

The results obtained for NLPC's of AR are consistent with those that were obtained by Montealegre [75] and Navarro et al. [76]. They reported a reduction (increase) in the monthly rainfalls linked to positive (negative) anomalies of the oceanic ENSO indices, mainly in the gauge stations of the Andean Zone, the northwest, and north regions of Colombia. These results are also coherent with those that were obtained in the studies of the relationship between the other hydro-climatic variables and large scale climate indices in Colombia [11,21,30,32]. In contrast, the results obtained for PR showed that the monthly rainfall in this region has a direct relationship with the oceanic climate indices, mainly Niño3 and Niño1 + 2. These results are consistent with those that were obtained by Montealegre [75].

They demonstrate a reduction (increase) in the rainfall of the Tumaco gauge station (located in PR) linked to negative (positive) values of these oceanic indices. The relationship between rainfall and oceanic climate indices registered in PR is similar to the connection found on the Ecuadorian coast; here, De Guennie et al. [67] showed a positive correlation between Niño1 + 2, and Niño3 and the rainfall anomalies at lag = 0.



**Figure 11.** Wavelet transforms coherence between the NLPC1-PR series and climate-oceanographic indices: (a) SST3 and (b) SOI. The closed contours indicate the squared Wavelet Coherence. The region where the edge effects are significant is under the cone of influence. The arrows denote phase differences: in-phase ( $0^\circ$ ), arrows point out to the right; out of phase ( $180^\circ$ ), arrows point out to the left; the first-time series leads the second by  $90^\circ$ , pointing down; and, the first-time series, the second one by  $90^\circ$ , pointing upwards.

With respect to the results of the cross-correlation analysis of the lagged effect to 12 months of the climate-oceanographic indices on rainfall in AR (PR), a strong (weak) persistence of up to six to 12 (five to 12) months was evidenced (See Figure 7). The results were consistent with Navarro et al. [77]. They indicate a lagged effect of up to 6–9 months regarding the relationship between the rainfalls in Western Colombia and the ENSO indices. In the same way, Canchala et al. [11] showed that the teleconnections between streamflows of two large rivers of the Choco Biogeographic Colombian and large scale climate indices are persistent for nine months. Moreover, this relationship was positive (negative) with atmospheric (oceanic) indices. Unlike the NLPC1-PR, the maximum correlations for the NLPC1-AR were obtained with the Niño indices (1 + 2, 3, 3.4, and 4) synchronously. Besides, the Niño3.4 and Niño4 influences on the AR rainfall were more substantial than the Niño1 + 2 and Niño3, which remained for another 10 and eight months, respectively. The result is coherent with the work developed by Poveda and Mesa [63]. They identified that Colombian precipitation has a higher correlation with the SST in the Niño4 region in the Central Pacific than other Niño regions close to SA.

In contrast, for NLPC1-PR, the strongest correlations with ENSO indices were recorded for Niño3.4 and Niño4 in 8, 9, and 10-lags (Figure 7c). Therefore, the ENSO influence occurred for 8, 9, and 10 months after the increase or decrease of SST in TPO. However, the findings indicate that the highest synchronous correlations depend on Niño1 + 2 and Niño3, which were positive, indicating a direct relationship. The influence of Niño1 + 2 is similar to that exerted on the rainfall of the neighboring country (Ecuador). It is directly influenced by SST in the waters near the shore (Niño1 + 2) [70]. On the other hand, AR and

PR showed positive relationships with the SOI index, and these were coherent with results that were registered by Ávila et al. [9], Canchala et al. [11], Poveda et al. [16], and Loaiza et al. [78]. The influence of the SOI index is higher in the AR than in the PR. Furthermore, the rainfall influence on the AR is almost synchronous (Lag 1), while the rainfall in PR is substantial in lags 8, 9, and 10.

Other findings show a statistically significant negative relationship between the PDO index and the NLPC1-AR with a maximum value for a nine-month lag (Figure 7a). A similar relationship was recorded between the streamflows of the two basins of the Choco Biogeographic Colombian by Canchala et al. [11]. According to Labat [79] and Shi et al. [80], ocean-atmospheric oscillations altogether enforce a strong influence on hydro-climatology; hence, climatic variability is subject to the joining and teleconnections of these large-scale processes. The PDO can change the periodicity of ENSO episodes according to the phase, which favoured the occurrence of lower (higher) rainfall, while positive EN/PDO (negative LN/PDO) episodes occur [81].

In summary, the rainfall in two-sub-regions of Southwestern Colombia showed significant differences in their spatio-temporal variability and their teleconnections with climate-oceanographic indices. When considering that climate indices showed high coherence (statistically significant), further study for the adequate management of water resources is suggested, since these can facilitate the prediction of monthly rainfall several months in advance.

#### 4. Conclusions

Using NLPCA, Pearson's Correlations, and Wavelet Analysis, in this research study, we were able to identify two sub-regions in southwestern Colombia: the Andean Region (AR) and Pacific Region (PR), in order to study their main variability time scales of the monthly rainfalls and their relationships with eight climate-oceanographic indices. Our findings are summarized, as follows:

1. From the NLPCA, we found two main modes of variability in AR and one in PR that explained around 75% and 48% of the variance of the original datasets, respectively. The positive (negative) periods of NLPC1-AR and NLPC2-AR coincided with the LN (EN) events. In contrast, those positive (negative) periods of NLPC1-PR coincided with EN (LN) events, i.e., the variability of monthly rainfall in the Andean region is contrary to the variability of monthly rainfall in the Nariño coastal region. The variability of monthly rainfall in AR is similar to the variability of rainfall in most of the Colombian territory, and the variability of monthly rainfall in PR is similar to the variability of rainfall that is registered in the coastal region of the border country, Ecuador.
2. The Pearson's Correlation between NLPCs of AR and PR and eight climate-oceanographic indices showed that the rainfall in AR has a direct (inverse) relationship with the SOI (ONI, MEI, Niño1 + 2, Niño3, Niño3.4, Niño4, and PDO) indices. Furthermore, the magnitude of the correlations was strongest with Niño3.4 and Niño4, and this influence remained for 10 and eight months, respectively. In this regard, the rainfall in PR showed positive synchronous correlations, but non-statistical significance with Niño1 + 2 and Niño3 indices, and an inverse relationship with Niño3.4 and Niño4 in 8, 9, and 10-lags. Overall, indices that were linked to the ENSO phenomenon showed strong teleconnections with the rainfall in AR, and weak ones in PR. The established results allow us to infer that the variability of rainfall in Southwestern Colombia influences the ENSO's inter-annual phenomenon its influence is stronger in east Nariño than on the west. These results are especially important for subsequent prediction analyses, given that the climate-oceanographic-indices with high synchronous and lagging correlation could become potential predictors of monthly rainfall in these sub-regions of Southwestern Colombia.
3. Wavelet Coherence analysis confirmed the relationships between ENSO indices and rainfall of AR and PR, which showed that the variability of the rain in AR is strongly influenced by the ENSO indices, mainly by the SST in the regions Niño3.4 and Niño4 on the 3–7-year inter-annual scale. Furthermore, this analysis ratified the weak influence of the ENSO phenomenon on PR rainfall. However, we noticed that, in the 1.5–3-year inter-annual scale, there is an influence of the SST in the region Niño3. Overall, the rain in AR is associated to the SST in the east TPO

(Niño3.4, Niño4, ONI, and MEI), where the warm (cold) phase of ENSO led to dry (wet) conditions for approximately 5–11 months. Meanwhile, the rainfall of PR is associated to the SST in the center of TPO (Niño3), where the warm (cold) phase of ENSO led to wet (dry) conditions for approximately 1–5 months.

4. The main findings of this research study are an understanding of the monthly variability rainfall in AR and PR, in Southwestern Colombia concerning the teleconnections with eight climate indices (when considering the multi-scale relations). This study allowed for us to establish for the first time the contrary relationships between ENSO indices and monthly rainfall in the sub-regions studied, where the EN events lead to a decrease (increase) in the monthly rainfall on AR (PR), while the opposite occurred in the LN events. The ENSO influence on the rainfall of the AR is highly correlated, and it has similar behavior to the impact of ENSO over most of the Colombian territory. In contrast, the findings revealed that the ENSO influence on PR is weak, showing similarities with the ENSO influence over the rainfall in the neighboring country of Ecuador. These results show that future studies need to explore the ocean-atmospheric and regional circulation processes that explain the marked difference in the relationships between ENSO and the region's rainfall.

**Author Contributions:** Conceptualization—T.C., W.A.-M., W.L.C., and Y.C.-E.; methodology—T.C., W.A.-M., and W.L.C.; T.C., W.A.-M., and W.L.C. managed the software; validation—T.C., W.A.-M., and W.L.C.; formal analysis—T.C., W.A.-M., W.L.C., and Y.C.-E.; investigation—T.C., W.A.-M., W.L.C., and Y.C.-E.; data curation—T.C., and W.A.-M.; original draft preparation—T.C., W.A.-M., W.L.C., and Y.C.-E.; reviewing and editing—T.C., W.A.-M., W.L.C., Y.C.-E., and E.C.-B.; visualization—T.C., W.A.-M., W.L.C., Y.C.-E., and E.C.-B.; supervision—W.A.-M., and Y.C.-E. All authors have read and agreed to the published version of the manuscript.

**Funding:** The first author was supported by the Program for Strengthening Regional Capacities in Research, Technological Development and Innovation in the department of Nariño and the CEIBA foundation for doctoral studies. The third author was supported by the Universidad del Valle (Cali-Colombia). The authors thank the Universidad del Valle for financing the research project CI 21010, and Colciencias for funding the research project “Análisis de eventos extremos de precipitación asociados a variabilidad y cambio climático para la implementación de estrategias de adaptación en sistemas productivos agrícolas de Nariño”.

**Conflicts of Interest:** The authors declare no conflict of interest. The founding sponsors had no role in the design, analysis, and interpretation of data, in the writing manuscript, or in the decision to publish the results.

## References

1. Coulibaly, P. Spatial and temporal variability of Canadian seasonal precipitation (1900–2000). *Adv. Water Resour.* **2006**, *29*, 1846–1865. [[CrossRef](#)]
2. Min, S.-K.; Zhang, X.; Zwiers, F.W.; Hegerl, G.C. Human contribution to more-intense precipitation extremes. *Nature* **2011**, *470*, 378–381. [[CrossRef](#)]
3. Xiao, M.; Zhang, Q.; Singh, V.P. Spatiotemporal variations of extreme precipitation regimes during 1961–2010 and possible teleconnections with climate indices across China. *Int. J. Climatol.* **2017**, *37*, 468–479. [[CrossRef](#)]
4. Schulte, J.A.; Najjar, R.G.; Li, M. The influence of climate modes on streamflow in the Mid-Atlantic region of the United States. *J. Hydrol. Reg. Stud.* **2016**, *5*, 80–99. [[CrossRef](#)]
5. Kim, T.; Shin, J.-Y.; Kim, S.; Heo, J.-H. Identification of relationships between climate indices and long-term precipitation in South Korea using ensemble empirical mode decomposition. *J. Hydrol.* **2018**, *557*, 726–739. [[CrossRef](#)]
6. Cai, W.; McPhaden, M.J.; Grimm, A.M.; Rodrigues, R.R.; Taschetto, A.S.; Garreaud, R.D.; Dewitte, B.; Poveda, G.; Ham, Y.-G.; Santoso, A. Climate impacts of the El Niño–Southern Oscillation on South America. *Nat. Rev. Earth Environ.* **2020**, *1*, 215–231. [[CrossRef](#)]
7. Montealegre, E.J.; Pabón, J.D. La variabilidad climática interanual asociada al ciclo El Niño-La Niña-Oscilación del Sur y su efecto en el patrón pluviométrico de Colombia. *Meteorol. Colomb.* **2000**, *2*, 7–21.
8. Poveda, G.; Jaramillo, A.; Gil, M.M.; Quiceno, N.; Mantilla, R.I. Seasonally in ENSO-related precipitation, river discharges, soil moisture, and vegetation index in Colombia. *Water Resour. Res.* **2001**, *37*, 2169–2178. [[CrossRef](#)]

9. Ávila, Javier, D.Á.; Carvajal Escobar, Y.; Gutiérrez Serna, S.E. Análisis de la influencia de El Niño y La Niña en la oferta hídrica mensual de la cuenca del río Cali. *Tecnura* **2013**, *18*, 120–133.
10. Poveda, G.; Vélez, J.; Mesa, O.; Hoyos, C.; Mejía, J.F.; Barco, O.J.; Correa, P.L. Influencia de fenómenos macroclimáticos sobre el ciclo anual de la hidrología colombiana: Cuantificación lineal, no lineal y percentiles probabilísticos. *Meteorol. Colomb.* **2002**, *6*, 121–130.
11. Canchala, T.; Loaiza Cerón, W.; Francés, F.; Carvajal-Escobar, Y.; Andreoli, R.V.; Kayano, M.T.; Alfonso-Morales, W.; Caicedo-Bravo, E.; Ferreira de Souza, R.A. Streamflow Variability in Colombian Pacific Basins and Their Teleconnections with Climate Indices. *Water* **2020**, *12*, 526. [[CrossRef](#)]
12. Loaiza, W.; Carvajal-Escobar, Y.; Andreoli, R.V.; Kayano, M.T.; Gonzáles, N. Spatio-temporal variability of the droughts in Cali, Colombia and their relationships with the El Niño-Southern Oscillation (ENSO) between 1971 and 2011. *Atmósfera* **2020**, *33*, 51–69. [[CrossRef](#)]
13. Jaramillo, L.; Poveda, G.; Mejía, J.F. Mesoscale convective systems and other precipitation features over the tropical Americas and surrounding seas as seen by TRMM. *Int. J. Climatol.* **2017**, *37*, 380–397. [[CrossRef](#)]
14. Yepes, J.; Poveda, G.; Mejía, J.F.; Moreno, L.; Rueda, C. CHOCO-JEX: A research experiment focused on the CHOCO low-level jet over the far Eastern Pacific and Western Colombia. *Bull. Am. Meteorol. Soc.* **2019**, *100*, 779–796. [[CrossRef](#)]
15. Espinoza, J.C.; Garreaud, R.; Poveda, G.; Arias, P.A.; Molina-Carpio, J.; Masiokas, M.; Viale, M.; Scaff, L. Hydroclimate of the Andes Part I: Main climatic features. *Front. Earth Sci.* **2020**, *8*, 64. [[CrossRef](#)]
16. Poveda, G.; Jaramillo, L.; Vallejo, L.F. Seasonal precipitation patterns along pathways of South American low-level jets and aerial rivers. *Water Resour. Res.* **2014**, *50*, 98–118. [[CrossRef](#)]
17. Poveda, G.; Mesa, O. La corriente de chorro superficial del Oeste (“del Chocó”) y otras dos corrientes de chorro en Colombia: Climatología y variabilidad durante las fases del ENSO”. *Rev. Acad. Colomb. Cienc.* **1999**, *23*, 517–528.
18. Vuille, M.; Bradley, R.S.; Keimig, F. Interannual climate variability in the Central Andes and its relation to tropical Pacific and Atlantic forcing. *J. Geophys. Res. Atmos.* **2000**, *105*, 12447–12460. [[CrossRef](#)]
19. Villacis, M.; Taupin, J.D. Variabilité climatique dans la sierra équatorienne en relation avec le phénomène ENSO. In Proceedings of the International Conference on Hydrology of the Mediterranean and Semi-Arid Regions, Montpellier, France, 1–4 April 2003; p. 202.
20. Hurtado, A. Estimación de los Campos Mensuales Históricos de Precipitación en el Territorio Colombiano. Master’s Thesis, Universidad Nacional de Colombia, Medellín, Colombia, December 2009.
21. Poveda, G.; Álvarez, D.M.; Rueda, Ó.A. Hydro-climatic variability over the Andes of Colombia associated with ENSO: A review of climatic processes and their impact on one of the Earth’s most important biodiversity hotspots. *Clim. Dyn.* **2011**, *36*, 2233–2249. [[CrossRef](#)]
22. Tootle, G.A.; Piechota, T.C.; Gutiérrez, F. The relationships between Pacific and Atlantic Ocean sea surface temperatures and Colombian streamflow variability. *J. Hydrol.* **2008**, *349*, 268–276. [[CrossRef](#)]
23. Rojo, J.D.; Carvajal, L.F. Predicción no lineal de caudales utilizando variables macroclimáticas y análisis espectral singular. *Tecnol. Cienc. Agua* **2010**, *1*, 59–73.
24. Rodríguez-Rubio, E. A multivariate climate index for the western coast of Colombia. *Adv. Geosci.* **2013**, *33*, 21–26. [[CrossRef](#)]
25. Córdoba-Machado, S.; Palomino-Lemus, R.; Gámiz-Fortis, S.R.; Castro-Díez, Y.; Esteban-Parra, M.J. Influence of tropical Pacific SST on seasonal precipitation in Colombia: Prediction using El Niño and El Niño Modoki. *Clim. Dyn.* **2015**, *44*, 1293–1310. [[CrossRef](#)]
26. Cuadrado, P.B.; Blanco, R.J. Teleconexiones y eventos extremos de sequía en áreas protegidas del norte de Colombia. *Rev. Climatol.* **2015**, *15*, 27–38.
27. Restrepo, J.C.; Higgins, A.; Escobar, J.; Ospino, S.; Hoyos, N. Contribution of low-frequency climatic–oceanic oscillations to streamflow variability in small, coastal rivers of the Sierra Nevada de Santa Marta (Colombia). *Hydrol. Earth Syst. Sci.* **2019**, *23*, 2379–2400. [[CrossRef](#)]
28. Canchala, T.; Carvajal-Escobar, Y.; Alfonso-Morales, W.; Loaiza, W.; Caicedo, E. Estimation of missing data of monthly rainfall in southwestern Colombia using artificial neural networks. *Data Br.* **2019**. [[CrossRef](#)]
29. Scholz, M.; Kaplan, F.; Guy, C.L.; Kopka, J.; Selbig, J. Non-linear PCA: A missing data approach. *Bioinformatics* **2005**, *21*, 3887–3895. [[CrossRef](#)]
30. Carvajal, Y.; Grisales, C.; Mateus, J. Correlación de variables macroclimáticas del Océano Pacífico con los caudales en los ríos interandinos del Valle del Cauca (Colombia). *Rev. Peru. Biol.* **1999**, *6*, 9–17. [[CrossRef](#)]

31. Poveda, G. La hidroclimatología de Colombia: Una síntesis desde la escala inter-decadal hasta la escala diaria. *Rev. Acad. Colomb. Cienc.* **2004**, *28*, 201–222.
32. Puertas, O.; Carvajal, Y.E. Incidence of El Niño southern oscillation in the precipitation and the temperature of the air in Colombia, using Climate Explorer. *Ing. Desarro.* **2008**, *23*, 104–118.
33. Wolter, K.; Timlin, M.S. El Niño/Southern Oscillation behaviour since 1871 as diagnosed in an extended multivariate ENSO index (MEI. ext). *Int. J. Climatol.* **2011**, *31*, 1074–1087. [[CrossRef](#)]
34. L’Heureux, M.L.; Collins, D.C.; Hu, Z.-Z. Linear trends in sea surface temperature of the tropical Pacific Ocean and implications for the El Niño–Southern Oscillation. *Clim. Dyn.* **2013**, *40*, 1223–1236. [[CrossRef](#)]
35. Mantua, N.J.; Hare, S.R.; Zhang, Y.; Wallace, J.M.; Francis, R.C. A Pacific interdecadal climate oscillation with impacts on salmon production. *Bull. Am. Meteorol. Soc.* **1997**, *78*, 1069–1080. [[CrossRef](#)]
36. Hsieh, W.W.; Tang, B. Applying neural network models to prediction and data analysis in meteorology and oceanography. *Bull. Am. Meteorol. Soc.* **1998**, *79*, 1855–1870. [[CrossRef](#)]
37. Kohonen, T.; Hynninen, J.; Kangas, J.; Laaksonen, J. *Som Pak: The Self-Organizing Map Program Package*; Report A31; Helsinki University of Technology, Laboratory of Computer and Information Science: Helsinki, Finland, January 1996.
38. Kohonen, T. *Self-Organizing Maps*; (Series in Information Sciences); Springer: Berlin/Heidelberg, Germany, 2001; Volume 30, p. 502. [[CrossRef](#)]
39. Kohonen, T. Self-organized formation of topologically correct feature maps. *Biol. Cybern.* **1982**, *43*, 59–69. [[CrossRef](#)]
40. Kalteh, A.M.; Hjorth, P.; Berndtsson, R. Review of the self-organizing map (SOM) approach in water resources: Analysis, modelling and application. *Environ. Model. Softw.* **2008**, *23*, 835–845. [[CrossRef](#)]
41. Lin, G.-F.; Chen, L.-H. Identification of homogeneous regions for regional frequency analysis using the self-organizing map. *J. Hydrol.* **2006**, *324*, 1–9. [[CrossRef](#)]
42. Chen, S.; Mangiameli, P.; West, D. The comparative ability of self-organizing neural networks to define cluster structure. *Omega* **1995**, *23*, 271–279. [[CrossRef](#)]
43. Fisher, R.A. The use of multiple measurements in taxonomic problems. *Ann. Eugen.* **1936**, *7*, 179–188. [[CrossRef](#)]
44. Pham, Q.B.; Yang, T.-C.; Kuo, C.-M.; Tseng, H.-W.; Yu, P.-S. Combing random forest and least square support vector regression for improving extreme rainfall downscaling. *Water* **2019**, *11*, 451. [[CrossRef](#)]
45. Shen, S.S.; Wied, O.; Weithmann, A.; Regele, T.; Bailey, B.A.; Lawrimore, J.H. Six temperature and precipitation regimes of the contiguous United States between 1895 and 2010: A statistical inference study. *Theor. Appl. Climatol.* **2016**, *125*, 197–211. [[CrossRef](#)]
46. Razi, T. A precipitation regionalization and regime for Iran based on multivariate analysis. *Theor. Appl. Climatol.* **2018**, *131*, 1429–1448. [[CrossRef](#)]
47. Hsieh, W.W. Nonlinear principal component analysis by neural networks. *Tellus A Dyn. Meteorol. Oceanogr.* **2001**, *53*, 599–615. [[CrossRef](#)]
48. Scholz, M. Validation of nonlinear PCA. *Neural Process. Lett.* **2012**, *36*, 21–30. [[CrossRef](#)]
49. Kenfack, C.S.; Mkankam, F.K.; Alory, G.; Du Penhoat, Y.; Houkonnou, M.N.; Vondou, D.A.; Nfor, G.B. Sea surface temperature patterns in the Tropical Atlantic: Principal component analysis and nonlinear principal component analysis. *Terr. Atmos. Ocean. Sci.* **2017**, *28*, 395–410. [[CrossRef](#)]
50. Scholz, M.; Vigário, R. Nonlinear PCA: A new hierarchical approach. In Proceedings of the 10th European Symposium on Artificial Neural Networks (ESANN), Bruges, Belgium, 24–26 April 2002; pp. 439–444.
51. Monahan, A.H. Nonlinear principal component analysis by neural networks: Theory and application to the Lorenz system. *J. Clim.* **1999**, *13*, 821–835. [[CrossRef](#)]
52. Monahan, A.H. Nonlinear principal component analysis: Tropical Indo–Pacific sea surface temperature and sea level pressure. *J. Clim.* **2001**, *14*, 219–233. [[CrossRef](#)]
53. Miró, J.J.; Caselles, V.; Estrela, M.J. Multiple imputation of rainfall missing data in the Iberian Mediterranean context. *Atmos. Res.* **2017**, *197*, 313–330. [[CrossRef](#)]
54. Razavi, T.; Coulibaly, P. An evaluation of regionalization and watershed classification schemes for continuous daily streamflow prediction in ungauged watersheds. *Can. W. Res. J./Rev. Can. Ressour. Hydri.* **2017**, *42*, 2–20. [[CrossRef](#)]
55. Rathinasamy, M.; Agarwal, A.; Sivakumar, B.; Marwan, N.; Kurths, J. Wavelet analysis of precipitation extremes over India and teleconnections to climate indices. *Stoch. Environ. Res. Risk Assess.* **2019**, *33*, 2053–2069. [[CrossRef](#)]

56. Coulibaly, P.; Burn, D.H. Wavelet analysis of variability in annual Canadian streamflows. *Water Resour. Res.* **2004**, *40*. [[CrossRef](#)]
57. Grinsted, A.; Moore, J.C.; Jevrejeva, S. Application of the cross wavelet transform and wavelet coherence to geophysical time series. *Nonlinear Process. Geophys.* **2004**, *11*, 561–566. [[CrossRef](#)]
58. Torrence, C.; Compo, G.P. A practical guide to wavelet analysis. *Bull. Am. Meteorol. Soc.* **1998**, *79*, 61–78. [[CrossRef](#)]
59. Torrence, C.; Webster, P.J. Interdecadal changes in the ENSO–monsoon system. *J. Clim.* **1999**, *12*, 2679–2690. [[CrossRef](#)]
60. Trenberth, K. The Climate Data Guide: Nino SST Indices (Nino 1+ 2, 3, 3.4, 4; ONI and TNI). 2019. Available online: <https://climatedataguide.ucar.edu/climate-data/nino-sst-indices-nino-12-3-34-4-oni-and-tri> (accessed on 6 September 2019).
61. Tedeschi, R.G.; Cavalcanti, I.F.; Grimm, A.M. Influences of two types of ENSO on South American precipitation. *Int. J. Clim.* **2012**, *33*, 1382–1400. [[CrossRef](#)]
62. Córdoba-Machado, S.; Palomino-Lemus, R.; Gámiz-Fortis, S.R.; Castro-Díez, Y.; Esteban-Parra, M.J. Assessing the impact of El Niño Modoki on seasonal precipitation in Colombia. *Glob. Planet. Chang.* **2015**, *124*, 41–61.
63. Poveda, G.; Mesa, O.J. Feedbacks between hydrological processes in tropical South America and large-scale ocean–atmospheric phenomena. *J. Clim.* **1997**, *10*, 2690–2702. [[CrossRef](#)]
64. Ávila, Á.; Guerrero, F.C.; Escobar, Y.C.; Justino, F. Recent Precipitation Trends and Floods in the Colombian Andes. *Water* **2019**, *11*, 379. [[CrossRef](#)]
65. Hoyos, N.; Escobar, J.; Restrepo, J.; Arango, A.; Ortiz, J. Impact of the 2010–2011 La Niña phenomenon in Colombia, South America: The human toll of an extreme weather event. *Appl. Geogr.* **2013**, *39*, 16–25. [[CrossRef](#)]
66. IDEAM. *Efectos Naturales y Socioeconómicos del Fenómeno El Niño en Colombia*; The Institute of Hydrology, Meteorology and Environmental Studies: Bogota, Colombia, 2002; p. 58.
67. De Guenni, L.B.; García, M.; Muñoz, A.G.; Santos, J.L.; Cedeño, A.; Perugachi, C.; Castillo, J. Predicting monthly precipitation along coastal Ecuador: ENSO and transfer function models. *Theor. Appl. Climatol.* **2017**, *129*, 1059–1073. [[CrossRef](#)]
68. Quishpe-Vásquez, C.; Gámiz-Fortis, S.R.; García-Valdecasas-Ojeda, M.; Castro-Díez, Y.; Esteban-Parra, M.J. Tropical Pacific sea surface temperature influence on seasonal streamflow variability in Ecuador. *Int. J. Climatol.* **2019**, *39*, 3895–3914. [[CrossRef](#)]
69. McPhaden, M.J.; Zebiak, S.E.; Glantz, M.H. ENSO as an integrating concept in earth science. *Science* **2006**, *314*, 1740–1745. [[CrossRef](#)] [[PubMed](#)]
70. Waylen, P.; Poveda, G. El Niño–Southern Oscillation and aspects of western South American hydro-climatology. *Hydrol. Process.* **2002**, *16*, 1247–1260. [[CrossRef](#)]
71. Poveda, G.; Waylen, P.R.; Pulwarty, R.S. Annual and inter-annual variability of the present climate in northern South America and southern Mesoamerica. *Palaeogeogr. Palaeoclimatol. Palaeoecol.* **2006**, *234*, 3–27. [[CrossRef](#)]
72. Mera, Y.E.Z.; Vera, J.F.R.; Pérez-Martín, M.Á. Linking El Niño Southern Oscillation for early drought detection in tropical climates: The Ecuadorian coast. *Sci. Total Environ.* **2018**, *643*, 193–207. [[CrossRef](#)]
73. Guzmán, D.; Ruíz, J.; Cadena, M. *Regionalización de Colombia Según la Estacionalidad de la Precipitación Media Mensual, a Través Análisis de Componentes Principales (acp)*; Grupo de Modelamiento de Tiempo, Clima y Escenarios de Cambio Climático, Subdirección de Meteorología–IDEAM: Bogota, Colombia, 2014.
74. Estupiñán, A.R. *Estudio de la Variabilidad Espacio Temporal de la Precipitación en Colombia*; Universidad Nacional de Colombia: Medellín, Colombia, 2016.
75. Montealegre, J. *Estudio de la Variabilidad Climática de la Precipitación en Colombia Asociada a Procesos Oceánicos y Atmosféricos de Meso y Gran Escala*; IDEAM: Bogota, Colombia, 2009.
76. Navarro, E.; Arias, P.A.; Vieira, S.C. El Niño–Oscilación del Sur, fase Modoki, y sus efectos en la variabilidad espacio-temporal de la precipitación en Colombia. *Rev. Acad. Colomb. Cienc. Exactas Fís. Nat.* **2019**, *43*, 120–132. [[CrossRef](#)]
77. Navarro, E.; Vieira, C.; Arias, P. Spatiotemporal variability of the precipitation in Colombia during ENSO events. In Proceedings of the XV Seminario Iberoamericano de Redes de Agua y Drenaje, (SEREA), Bogota, Colombia, 27–30 November 2017.

78. Loaiza Cerón, W.; Andreoli, R.V.; Kayano, M.T.; Ferreira de Souza, R.A.; Jones, C.; Carvalho, L. The Influence of the Atlantic Multidecadal Oscillation on the Choco Low-Level Jet and Precipitation in Colombia. *Atmosphere* **2020**, *11*, 174. [[CrossRef](#)]
79. Labat, D. Cross wavelet analyses of annual continental freshwater discharge and selected climate indices. *J. Hydrol.* **2010**, *385*, 269–278. [[CrossRef](#)]
80. Shi, P.; Yang, T.; Xu, C.-Y.; Yong, B.; Shao, Q.; Li, Z.; Wang, X.; Zhou, X.; Li, S. How do the multiple large-scale climate oscillations trigger extreme precipitation? *Glob. Planet. Chang.* **2017**, *157*, 48–58. [[CrossRef](#)]
81. Kayano, M.T.; Andreoli, R.V. Clima da Região Nordeste do Brasil. In *Tempo e Clima no Brasil*; Cavalcanti, I., Ferreira, N., Silva, M., Dias, M., Eds.; Oficina de Textos: São Paulo, Brazil, 2009.



© 2020 by the authors. Licensee MDPI, Basel, Switzerland. This article is an open access article distributed under the terms and conditions of the Creative Commons Attribution (CC BY) license (<http://creativecommons.org/licenses/by/4.0/>).